Thermal and Stress Modeling of Laser Fabrication of Multiple Material Components

K. Dai and L. Shaw
Department of Metallurgy and Materials Engineering
Institute of Materials Science
University of Connecticut, Storrs, CT 06269

ABSTRACT

Solid freeform fabrication (SFF) is an automated manufacturing process that builds three-dimensional complex-shaped structures layer-by-layer directly from CAD data without part-specific tooling and human intervention. In many cases multiple materials are involved in fabricating one component using SFF approaches. Porcelain-fused-to-metal (PFM) restoration for permanent fixed prosthodontics is an example of this kind. In this study 3-dimensional finite element modeling has been carried out to investigate the temperature and stress field in processing of multiple material components using a moving laser beam. Effects of fabrication sequences, laser scanning patterns and scanning rates on residual stresses have been investigated. Implications of these results on laser fabrication of multiple materials have been discussed.

Keywords: Solid freeform fabrication, Dental restoration, Laser processing, Finite element modeling, Thermal and stress analyses.

INTRODUCTION

Solid freeform fabrication (SFF) is an emerging manufacturing technology that creates 3-dimensional components directly from a CAD design without part-specific tooling and human intervention [1]. The development in SFF has offered opportunities to make the dental restoration using a SFF process with laser-assisted densification of multiple materials, or in short, multi-material laser densification (MMLD) [2]. In this process, dental restorations are built driectly from 3-D computer solid models through two steps. First, dental ceramic and metallic powders are delivered through slurry approaches point-by-point to the desired location. Second, once a layer (or a layer segment) is delivered, the layer is densified using a laser beam scanning in the desired pattern and with adjusted input power density depending on which powder material is under densification. After densification, a new layer of powders will be deposited as described in the first step, which will then be followed again by the second step. This layer-by-layer fabrication process continues until dental restoration is completed. The automation of the MMLD process offers opportunities to reduce the labor cost and increase the dental restoration rate.

For a specific restoration, many experiments are needed to optimize the fabrication process so that the maximum strength, minimum residual stress and distortion can be achieved. Such an experimental trial-and-error approach will inevitably lead to a high cost of the dental restoration through the MMLD process. Instead of using experimental trial-and-error approaches, this study uses finite element modeling (FEM) to investigate the effect of various processing parameters and to provide guidance for intelligent selection of various parameters in the MMLD process.

Finite element models were developed before to optimize several SFF processes for minimal residual thermal stresses and distortion in the final component fabricated. These efforts [3-11] provide substantial insights into how thermal gradients, thermal transient stresses and residual stresses in the fabrication of complex-shaped components using SFF processes. However, most of these models are limited to 1D or 2D cases [3-9] and all of them only deal with processing of single material [3-11]. In contrast, the present study provides 3-dimensional analyses of laser processing of components made of multiple materials. Furthermore, although the principal motivation for this work is to provide guidance for minimizing residual thermal stresses and distortion in the component fabricated via the MMLD process, the understanding developed in this work is expected to be applicable to other SFF processes that are involved with multiple materials. The result of this study may also be applied to conventional fabrication processes that are involved with heating of multi-material components using a moving laser source.

MODEL DESCRIPTION

To develop fundamental understanding on how temperature and stress gradients develop during laser processing of multiple materials and to evaluate the dependency of the thermal and stress fields on various laser processing parameters and material properties, bi-material laser processing with simple geometry has been investigated in this study. All of the models investigated have the same geometry. One of the models investigated is shown in Figure 1.

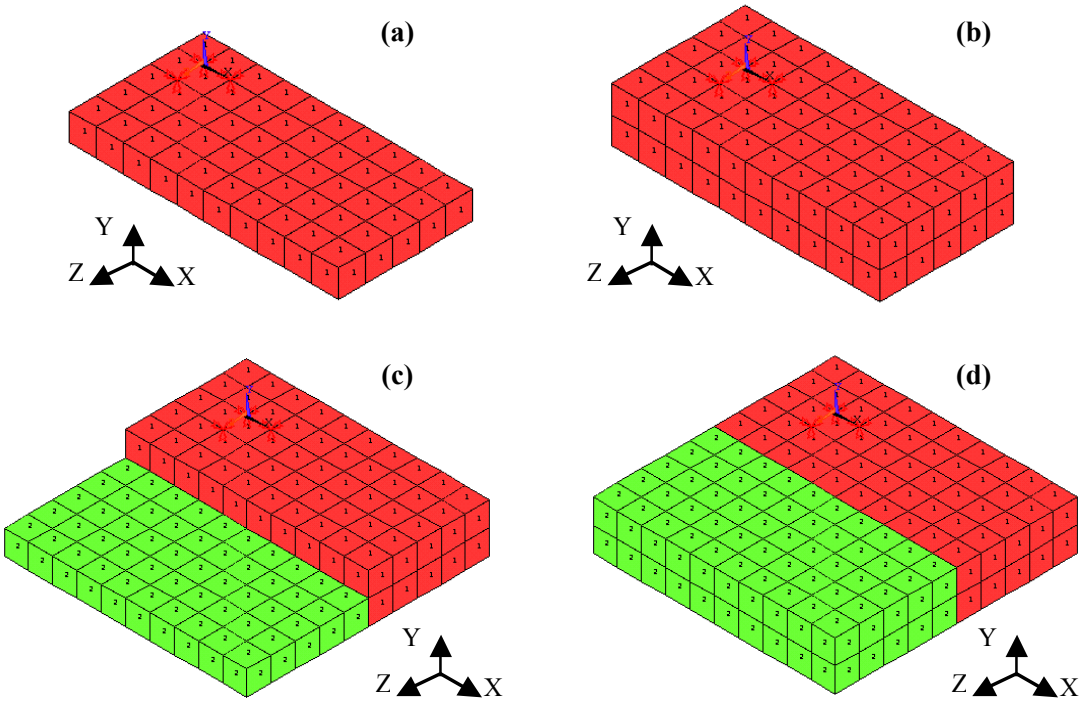

Figure 1. Schematic of fabrication sequence I. The dental alloy section (in dark color) is first fabricated in (a) and (b) steps, whereas the porcelain section (in gray color) is fabricated in (c) and (d) steps.

The model consists of a dental porcelain section (shown in gray color) and a dental nickel alloy section (shown in dark color). The final size of the part is 20×20×4 mm and the size of

every element in the mesh is 2×2×2 mm. The part is built layer-by-layer with two different laser fabrication sequences. Fabrication sequence I fabricates 3-dimensional bi-material bodies via buildup of the dental alloy section first, followed by buildup of the dental porcelain section, as shown in Figure 1. In contrast, fabrication sequence II entails fabrication of a 3-dimensional bi-material body through buildup of the bi-material layer-by-layer, as shown in Figure 2. For both fabrication sequences, all the elements in one layer are added simultaneously as the first layer, or onto the previous layer, or adjacent to the neighboring section built in the previous step depending on which step it is in the fabrication sequence. These elements are then subjected to laser processing (i.e., laser melting and solidification). After laser processing, a new layer of elements is added, which is then followed by laser processing. This element-adding and laser-processing procedure is to mimic the MMLD process described in the Introduction section.

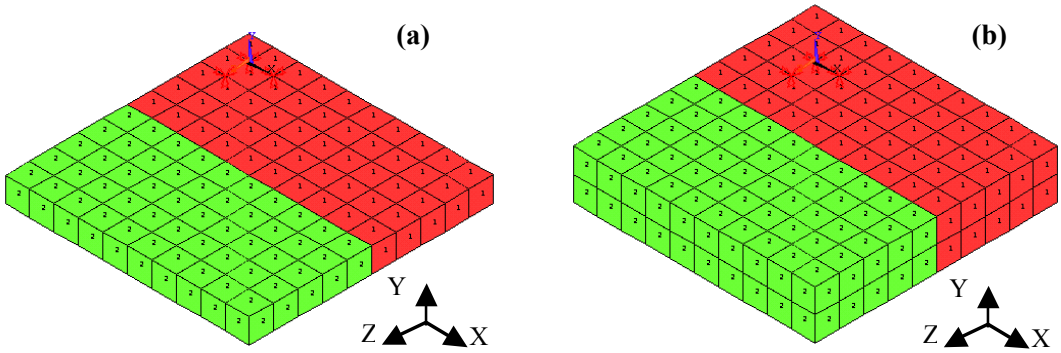

Figure 2. Schematic of fabrication sequence II. The first bi-material layer is fabricated in step (a), and the second bi-material layer is built in step (b).

For each fabrication sequence, two laser scanning patterns and two scanning rates have been investigated. The two scanning patterns for each fabrication sequence are shown in Figure 3. Note that scanning pattern A has its major scanning direction (i.e. the long scanning direction) parallel to the interface of the bi-material, whereas scanning pattern B has its major scanning direction perpendicular to the interface of the bi-material. The two scanning rates investigated are 10 and 100 μm/s. The combination of two fabrication sequences, two scanning patterns and two scanning rates results in a total of eight laser fabrication conditions all of which have been investigated and are complied in Table 1.

In simulation the dental nickel alloy is assumed to be pure nickel, while the dental porcelain is composed of 63.40% SiO_2, 16.70% Al_2O_3, 1.50% CaO, 0.80% MgO, 3.41% Na_2O, and 14.19% K_2O (wt%). The nickel has plastic deformation capacities and simulated using the bilinear kinematic hardening behavior. Furthermore, this bilinear kinematic hardening behavior is a function of temperature. The porcelain is assumed to be an elastic material below its melting point (1373K) and no fracture is considered. Above the melting temperature the behaviors of both the nickel and porcelain are approximated using plasticity with extremely low elastic moduli, tangent moduli and yield strengths. Such approximation maintains the fluidity of the molten nickel and porcelain although time-dependent properties (e.g., creep and viscous flow) are ignored. The numerical simulation is carried out using the ANSYS code [12]. The simulation approach, which has been crosschecked with analytical solutions for relatively simple geometry [13], has been used in this study. Every element in the model is assumed to be initially solid. The

latent heat of fusion is not considered in the model, nor is the volume change associated with melting and solidification. The latent heat of fusion and the volume change, especially those associated with powder densification, are expected to have influence on the transient and residual stresses and will be investigated in future studies. The model does not include the convection of liquid in the molten pool. This approximation is quite reasonable because the present simulation shows that the size of the molten pool generated under the assumed processing condition is similar to the size of the laser beam (~ 2 mm) and thus liquid convection if any will be very limited in such a small liquid pool.

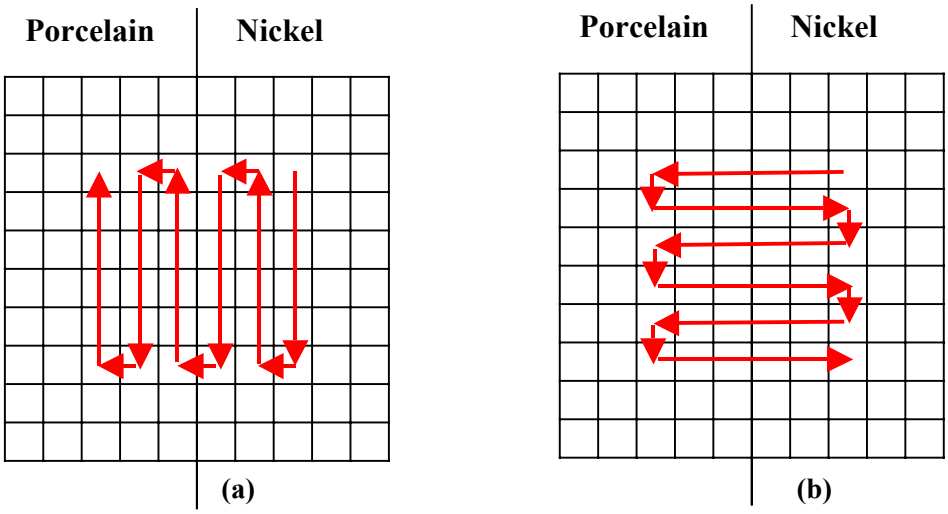

Figure 3. The two laser scanning patterns: (a) scanning pattern A and (b) scanning pattern B.

Table 1. Laser Densification Conditions Modeled

Model ID	Model 1	Model 2	Model 3	Model 4	Model 5	Model 6	Model 7	Model 8
Densification Sequence	I	I	I	I	II	II	II	II
Scanning Pattern	A	A	B	B	A	A	B	B
Scanning Rate (μm/s)	10	100	10	100	10	100	10	100

The boundary conditions for modeling are set as follows. The part being built is assumed to be in contact with air and the heat loss through air is approximated through the inclusion of a convection heat transfer coefficient (6×10^{-5} w/mm^{2}K) between the part and the ambient air. The ambient air is assumed to be 300K and the temperature dependence of the convection heat transfer coefficient is neglected. The laser beam heating is modeled as a fixed temperature and moves from a group of surface nodes within the laser beam size of 2×2 mm to the next group of surface nodes as defined by the fabrication sequence, the scanning pattern and the scanning rate. Such a heating condition mimics the temperature close-loop control used in the MMLD process [2]. The input temperature is set at 1740K when the laser beam scans in the nickel section and 1380K in the porcelain section and at the bi-material interface. To avoid rotation and translation of the part during simulation, the node at one of the bottom corners of the part is fixed in the x, y and z directions. Furthermore, the node next to the fixed node and located at the x-axis is fixed in the y and z directions, while the node next to the fixed node and located at the z-axis is fixed in the x and y directions. Fixing only one corner allows the part to respond to thermal transient and

residual stresses with minimum interference from the boundary condition, and thus stress and distortion analyses can be carried out with reasonable accuracy.

SIMULATION RESULTS AND DISCUSSION

Effects of Laser Scanning Patterns: The simulation results of Models 1 to 8 are summarized in Table 2 from which the effect of the scanning pattern can be found. For example, comparisons can be made among models with fabrication sequence I (Models 1 to 4). By comparing Models 1 (pattern A, 10 μm/s) with 3 (pattern B, 10 μm/s) and 2 (pattern A, 100 μm/s) with 4 (pattern B, 100 μm/s), we can conclude that pattern B generates larger residual stresses and thus larger distortion than pattern A. Recall that pattern A has the major laser scanning direction parallel to the interface (Figure 3a), while pattern B has the major laser scanning direction perpendicular to the interface (Figure 3b). The multiple heating and cooling cycles at the interface caused by scanning pattern B have resulted in large residual stresses and thus large distortion of the part. In contrast, for scanning pattern A the interfacial region is only heated once. Furthermore, such heating is followed by relatively slow cooling because of the subsequent laser processing of the neighboring porcelain region away from the interface. The slow cooling at the interfacial region has resulted in a small temperature gradient and thus low residual stresses and distortion.

Table 2. Summary of Simulation Results

Model ID	Temperature range of the part when the laser beam is scanning the final point (K)	Stress range of the part after cooling down to room temperature (MPa)		
		X-direction	Y-direction	Z-direction
1	379 ~ 1380	-288 ~ 543	-250 ~ 314	-319 ~ 67
2	463 ~ 1380	-310 ~ 552	-293 ~ 353	-346 ~ 109
3	565 ~ 1380	-336 ~ 548	-325 ~377	-486 ~ 95
4	494 ~ 1380	-350 ~ 563	-338 ~ 385	-460 ~ 112
5	379 ~ 1380	-447 ~ 579	-453 ~ 455	-431 ~ 152
6	464 ~ 1380	-439 ~ 614	-407 ~ 460	-425 ~ 184
7	927 ~ 1740	-441 ~ 593	-513 ~ 467	-480 ~ 236

Effects of Laser Scanning Rates: Effects of laser scanning rates can also be found in Table 2. For example, a comparison can be made between Models 1 and 2. Model 1 has a laser scanning rate of 10 μm/s, whereas Model 2 is 100 μm/s. Both of these models have the same scanning pattern (i.e., pattern A). The comparison indicates that both residual tensile and compressive stresses increase with scanning rate. More specifically, depending on which stress is concerned, the maximum tensile stress has risen by 2 to 62% and the maximum compressive stress has increased by 8 to 17% when the scanning rate increases from 10 to 100 μm/s. Corresponding to the increase in residual stresses, the distortion of the part has also increased by about 10%. However, when the comparison is made between Models 3 and 4 that have scanning pattern B, the result becomes more complex. Although the maximum residual tensile stress also increases with scanning rate (2 to 18% increase in the stress for a 10-times increase in the scanning rate), the maximum compressive stress may increase or decrease depending on which stress component is concerned (see Table 2). Such a complicated situation is also found in the comparisons between Models 5 and 6 and between Models 7 and 8. Thus, whether residual

stresses increase or decrease with increasing scanning rate depends on the scanning pattern and the stress component under consideration. No general rule can be made.

A close examination of Table 2 further reveals that the dependence of residual thermal stresses on scanning rates is also affected by the fabrication sequence. As will be discussed in the next section, the fabrication sequence II is not an acceptable fabrication sequence. Thus, as far as the fabrication sequence I is concerned, the x-stress, which is dominated by the CTE mismatch between the dental alloy and porcelain, always increases with scanning rate. This is related to the phenomenon that there is less time for the interface porcelain to expose to high temperatures when the scanning rate is high. As a result, the interface porcelain has shorter time in the molten state and thus less compressive permanent deformation. Such a smaller permanent compressive deformation of the porcelain in the molten state leads to a higher residual compressive x-stress in the porcelain and a higher tensile x-stress in the nickel because the nickel has a larger CTE and is constrained by the porcelain that has a less compressive deformation in its molten state. The same reasoning can be applied to the residual y-stress because the y-stress is also predominately controlled by the thermal mismatch between the dental alloy and porcelain.

Effects of Fabrication Sequences: The fabrication sequence has the largest effect on residual stresses and distortion among all the parameters we have evaluated. It also has substantial impacts on the transient stresses and temperature. It is noted from Table 2 that for fabrication sequence II with scanning pattern A (i.e., Models 5 and 6), the final temperature range of the part before it cools down to room temperature is close to that for fabrication sequence I with scanning pattern A (Models 1 and 2). However, if the transient temperature is examined (not shown in Table 2), it immediately becomes obvious that fabrication sequence II is not acceptable for fabricating a part with controlled shape and dimensions.

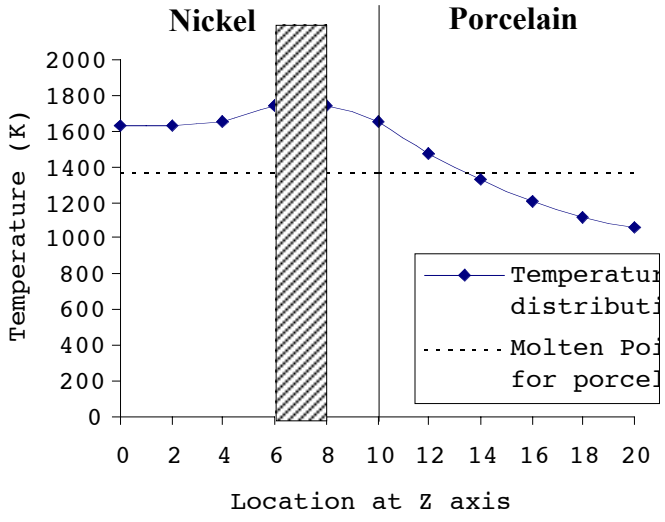

Figure 4. The temperature distribution along the nodal points with y = 4 and 0 ≤ z ≤ 20 at the y-z plane with x = 10 for Model 5 (i.e., fabrication sequence II, scanning pattern A and scanning rate 10 μm/s) when the laser beam is scanning the nickel alloy section. The hatched area indicates the location of the laser beam.

The point made above can be well illustrated using Figure 4 that shows the temperature distribution along the nodal points with y = 4 and 0 ≤ z ≤ 20 at the y-z plane with x = 10 for an

intermediate step of fabrication sequence II with scanning pattern A and a scanning rate of 10 μm/s (Model 5). It can be seen that the porcelain near the interface has temperatures higher than its melting point even though the laser beam is scanning at the neighboring nickel section before it reaches the porcelain section. Clearly, this is due to the high thermal conductivity of the dental nickel alloy and the high fabrication temperature (slightly higher than the melting point of the dental nickel alloy) used to process the nickel section. This result suggests that if fabrication sequence II is used for dental restoration, the shape and dimension of the porcelain section would be very difficult to control because the porcelain section have become liquid and led to substantial distortion of the shape even before the laser beam reaches the porcelain section. Models 7 and 8 suffer from the same problems as Models 5 and 6. Thus, when the melting points of the two materials are substantially different, fabrication sequence II is not an acceptable fabrication sequence.

CONCLUDING REMARKS

Processing of bi-material parts via a moving laser beam has been investigated using finite element modeling in this study. The effects of various processing parameters, including the fabrication sequence, laser scanning pattern and scanning rate, on the transient temperature, transient stresses, residual stresses and distortion of the part have been evaluated. Based on these investigations, the following conclusions can be offered.

1) Fabrication sequence I, which fabricates the section of the high melting temperature material (e.g., the dental nickel alloy) first and then the section of the low melting temperature material (e.g., the dental porcelain), is the appropriate sequence to fabricate the part made of two materials with the substantially different melting points. Fabrication sequence II, which fabricates the entire bi-material layer one after another, offers little control over the shape and dimension of the section of the low melting temperature material, and thus is not an acceptable fabrication sequence.
2) The transient thermal stresses generated using fabrication sequence I are relatively small and will not impose threats to the mechanical integrity of the part being fabricated (i.e., cracking in the dental porcelain section).
3) Thermal residual stresses are large in the direction along which shrinkage is strongly affected by the CTE mismatch between the two materials, and small in the direction along which shrinkage can take place with little influence from the CTE mismatch.
4) In general, using the fabrication sequence I the thermal residual stress and distortion increase with the laser scanning rate because the faster the scanning rate, the less permanent compressive deformation occurs to the molten porcelain. As a result of the less compressive deformation of the porcelain in its molten state, higher residual thermal compressive stresses appear in the interface porcelain and higher residual tensile stresses occur in the interface nickel.
5) Scanning pattern A with the major scanning direction parallel to the interface of the bi-material generates lower residual thermal stresses than scanning pattern B that has its major scanning direction perpendicular to the interface.
6) Effects of the fabrication sequence, laser scanning pattern and scanning rate are interrelated. The optimal combination of these parameters for fabricating bi-material parts with minimum residual stresses and distortion is fabrication sequence I, scanning pattern A and fast scanning rate.

Acknowledgements – The authors gratefully acknowledge financial support provided by the National Science Foundation under Grant No: DMI-9908249.

REFERENCES

1. Beaman, J.J., Barlow, J.W., Bourell, D.L., Crawford, R.H., Marcus, H.L. and McAlea, K.P., "Solid Freeform Fabrication: A New Direction in Manufacturing," Kluwer Academic Publishers, MA, 1997.
2. Li, X., Crocker, J., Geiss, E., Shaw, L., Marcus, H. and Cameron, T., "Evaluation of Microstructure and Properties for Multi-Materials Laser Densification of Dental Restorations," in the proceedings of the 11th Annual SFF Symposium, edited by D. L. Bourell, et al., The University of Texas, 2000, pp. 159 – 167.
3. Chin, R.K., Beuth, J.L. and Amon, C.H., "Thermomechanical Modeling of Molten Metal Droplet Solidification Applied to Layered Manufacturing," Mech. Mater., Vol. 24, 1996, pp. 257-271.
4. Amon, C.H., Beuth, J.L., Merz, R., Prinz, F.B. and Weiss, L.E., "Shape Deposition Manufacturing with Microcasting: Processing, Thermal and Mechanical Issues," J. Manufact. Sci. Eng., Vol. 120, No. 3, 1998, pp. 656-665.
5. Ong, R., Beuth, J.L. and Weiss, L.E., "Residual Stress Control Issues for Thermal Deposition of Polymers in SFF Processes," in the proceedings of the 11th Annual SFF Symposium, edited by D. L. Bourell, et al., The University of Texas, 2000, pp. 209-218.
6. Vasinonta, A., Beuth, J.L. and Griffith, M.L., "Process Maps for Controlling Residual Stress and Melt Pool Size in Laser-Based SFF Processes," in the proceedings of the 11th Annual SFF Symposium, edited by D. L. Bourell, et al., The University of Texas, 2000, pp. 200-208.
7. M. Kandis and T. L. Bergman, "A Simulation-Based Correlation of the Density and Thermal Conductivity of Objects Produced by Laser Sintering of Polymer Powders," J. Manufact. Sci. Eng., Vol. 122, No. 3, 2000, pp. 439-444.
8. Steinberger, J., Shen, J., Manetsberger, K. and Muellers, J., "The Simulation of the SLS Process as the Basis of a Process Optimization," in the proceedings of the 11th Annual SFF Symposium, edited by D. L. Bourell, et al., The University of Texas, 2000, pp. 377-385.
9. Zhang, Y and Faghri, A., "Melting of a Subcooled Mixed Powder Bed with Constant Heat Flux Heating," Int. J. Heat Mass Transfer, Vol. 42, 1999, pp. 775-788.
10. Childs, T.H.C., Hauser, C., Taylor, C.M. and Tontowi, A.E., "Simulation and Experimental Verification of Crystalline Polymer and Direct Metal Selective Laser Sintering," in the proceedings of the 11th Annual SFF Symposium, edited by D. L. Bourell, et al., The University of Texas, 2000, pp.100-109.
11. Bugeda, G., Cervera, M. and Lombera, G., "Numerical Prediction of Temperature and Density Distribution in Selective Laser Sintering Process," Rapid Prototyping J., Vol. 5, 1999, pp. 21-26.
12. ANSYS User's Manual, Vol. I-VI, Swanson Analysis Systems, Inc., Houston, PA, 1992.
13. Dai, K., Klemens, P. and Shaw, L., "Numerical Simulation of Bi-Materials Laser Densification," in the proceedings of the 11th Annual SFF Symposium, edited by D. L. Bourell, et al., The University of Texas, 2000, pp. 386-392.